A wave finite element strategy based on time of flight analysis to localize defects in networks of pipes

Diego Salam Claro, Vivien Denis, Jean-Mathieu Mencik

A wave finite element strategy based on time of flight analysis to localize defects in networks of pipes

D.S. Claro, V. Denis, J.-M. Mencik
INSA Centre Val de Loire, Université d'Orléans, Université de Tours, LaMé
Rue de la Chocolaterie, 41000 Blois, France
e-mail: **diego.salam_claro@insa-cvl.fr**

Abstract
A wave finite element (WFE) strategy to predict and localize defects in networks of straight pipes with curved joints is proposed. This involves estimating the times of flight taken by some narrow wave packets to get transmitted through or reflected by a coupling element that could represent either a joint or a defect. The ansatz proposed here is to define these times of flight from the frequency derivatives of the arguments of the scattering matrix of the coupling element. Also, the times of flight taken by wave packets to travel along a certain pipe can be classically obtained from the analysis of the group velocities. By comparing the theoretical expressions of the times of flight with those recorded in a network of pipes at some measurement point, it becomes possible to localize a defect with accurate precision and, also, to have a physical insight about the kind of waves which are transmitted through a joint and reflected by a defect (pathways). Numerical experiments are carried out which highlight the relevance and applicability of the proposed approach.

1 Introduction

Non-destructive testing usually involves generating guided waves and measuring reflected signals at some measurement points. For waveguides like pipes, straight beams or periodic structures, waves can travel a long distance and are usually sensitive to the presence of local defects and inhomogeneities [1]. However, the presence of curved joints can strongly penalize the detection of a defect by a certain kind of waves. This is due to wave mode conversion effects, i.e. a certain incident wave packet usually gives rise to several scattered wave packets of different natures.

The wave propagation in straight pipes has been extensively explored in the literature, see for instance [2, 3, 4]. Demma et al. [5] have investigated, numerically and experimentally, the transmitted/reflected wave signals in two pipes connected with a curved joint. Hayashi et al. [6] have applied the semi-analytical finite element method to analyze the propagation of axisymmetric modes in the presence of multiple curved joints, and the related transmitted/reflected energy flows. Sanderson et al. [7] have investigated the localization of a defect in a pipeline with a curved joint. They have shown that the defect localization can be prone to inaccurate results due to the presence of the curved joint. Finally, Ni et al. [8] have studied, numerically and experimentally, the signal issued from a defect beyond joints of different configurations.

In this work, the wave finite element (WFE) method is used as an efficient and straightforward alternative to predict and localize defects in pipes with curved joints. The method has been developed originally to compute the wave propagation in 1D periodic structures [9, 10, 11]. Later on, it has been applied to analyze periodic structures connected with a defect (coupling element) and determine the related wave reflection/transmission coefficients [12, 13, 14]. The strategy involves computing a scattering matrix from the finite element (FE) model of a coupling element and the incident/reflected waves in the connecting periodic structures (WFE) [11]. Results about defect localization in pipes can be found in [15, 16]. More recently in [17], a generalized scattering matrix model combining defect and joint FE models, and waveguide WFE models, has been proposed to optimize the joint properties and improve the detection of a defect.

In order to localize a defect, a time response analysis based on the study of the times of flight, for reflected or transmitted wave packets, can be used [18]. For straight pipes, assessing the times of flight follows directly from the analysis of the group velocities. However, assessing the group velocities for waves transmitted or reflected through arbitrary coupling elements, like defects or curved joints, is more dubious. To address this issue, it is proposed to define these times of flight from the frequency derivatives of the arguments of the scattering matrix of a coupling element. The scattering matrix results from FE/WFE modeling and enables the identification of the wave conversion effects through the coupling element. In other words, the proposed approach intends to predict the pathways, and the related times of flight, followed by a certain wave packet when it is transmitted or reflected by a coupling element. For a given incident wave packet, different types of reflected wave packets can be predicted since different pathways can be considered (coupling element). Fortunately, a fitting procedure with the experimental wave signals can help identify those different pathways and, further, the position of the defect.

The paper is organized as follows. In Section 2, the WFE method is briefly presented and the concept of time of flight through an arbitrary coupling element is developed. Also, the strategy to localize a defect in a network of pipes is presented. In Section 3, numerical experiments are brought concerning three pipes with a curved joint and a small defect in order to validate and highlight the accuracy of the proposed approach.

2 WFE method

2.1 Substructure modeling

The propagation of waves along straight pipes is investigated. Within the WFE framework, periodic structures composed of identical substructures with similar FE meshes are considered. For instance, a straight pipes composed of substructures of length d is shown in Fig. 1.

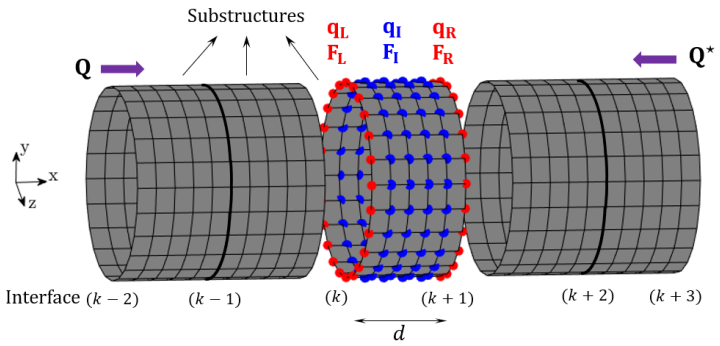

Figure 1: Schematic of a pipe described from identical substructures (periodic mesh).

Let us consider the FE model of a substructure, and let us denote by $\mathtt{L}/\mathtt{R}$ the degrees of freedom (DOFs) of the left/right boundary of this substructure, and by $\mathtt{I}$ the internal (i.e., the other) DOFs. Also, let us denote by n the number of DOFs on the left/right boundary, and by $\mathbf{M}$, $\mathbf{C}$ and $\mathbf{K}$ the mass, damping, and stiffness matrices of the substructure (respectively). In the frequency domain, the dynamic equilibrium equation of this substructure is given by:

$$\mathbf{D}\mathbf{q} = \mathbf{F}, \tag{1}$$

where $\mathbf{q}$ and $\mathbf{F}$ are the displacement and force vectors, respectively, and $\mathbf{D}$ is the dynamic stiffness matrix (DSM):

$$\mathbf{D} = -\omega^2\mathbf{M} + \mathtt{i}\omega\mathbf{C} + \mathbf{K}, \tag{2}$$

where ω is the angular frequency, and $\mathtt{i}$ is the imaginary unit. Although not mandatory, a Rayleigh-type damping matrix $\mathbf{C}$ can be considered, i.e.,

$$\mathbf{C} = a\mathbf{M} + b\mathbf{K}, \tag{3}$$

where a and b are two real positive constants. Following the WFE procedure, the following transfer matrix equation can be obtained from Eq. (1) [9, 11]:

$$\mathbf{u}_{\mathtt{R}} = \mathbf{S}\mathbf{u}_{\mathtt{L}}, \tag{4}$$

where

$$\mathbf{u}_{\mathtt{R}} = \begin{bmatrix} \mathbf{q}_{\mathtt{R}} \\ \mathbf{F}_{\mathtt{R}} \end{bmatrix}, \qquad \mathbf{u}_{\mathtt{L}} = \begin{bmatrix} \mathbf{q}_{\mathtt{L}} \\ -\mathbf{F}_{\mathtt{L}} \end{bmatrix}. \tag{5}$$

In Eq. (4), $\mathbf{S}$ is the transfer matrix of the substructure (size $2n \times 2n$) given by:

$$\mathbf{S} = \begin{bmatrix} -\mathbf{D}_{\mathtt{LR}}^{*-1}\mathbf{D}_{\mathtt{LL}}^{*} & -\mathbf{D}_{\mathtt{LR}}^{*-1} \\ \mathbf{D}_{\mathtt{RL}}^{*} - \mathbf{D}_{\mathtt{RR}}^{*}\mathbf{D}_{\mathtt{LR}}^{*-1}\mathbf{D}_{\mathtt{LL}}^{*} & -\mathbf{D}_{\mathtt{RR}}^{*}\mathbf{D}_{\mathtt{LR}}^{*-1} \end{bmatrix}, \tag{6}$$

where $\mathbf{D}^{*}$ is the condensed DSM of the substructure [19]. Two consecutive substructures can be coupled by imposing the equilibrium of the internal forces and the continuity of the displacements at the interfaces. This yields:

$$\begin{bmatrix} \mathbf{q}_{\mathtt{L}}^{(k+1)} \\ -\mathbf{F}_{\mathtt{L}}^{(k+1)} \end{bmatrix} = \mathbf{S} \begin{bmatrix} \mathbf{q}_{\mathtt{L}}^{(k)} \\ -\mathbf{F}_{\mathtt{L}}^{(k)} \end{bmatrix} \qquad \text{or} \qquad \begin{bmatrix} \mathbf{q}_{\mathtt{R}}^{(k+1)} \\ \mathbf{F}_{\mathtt{R}}^{(k+1)} \end{bmatrix} = \mathbf{S} \begin{bmatrix} \mathbf{q}_{\mathtt{R}}^{(k)} \\ \mathbf{F}_{\mathtt{R}}^{(k)} \end{bmatrix}, \tag{7}$$

where (k) and $(k+1)$ denotes two consecutive substructure interfaces, see Fig. 1.

The transfer matrix relation between two consecutive substructures is given by Eq. (7). It is well known that the eigensolutions of the matrix $\mathbf{S}$ represent waves. Its eigenvalues represent the wave parameters and are given by $\mu_j = \mathtt{exp}(-\mathtt{i}\beta_j d)$ where β_j denotes wavenumbers. Also, its eigenvectors represent the "cross-section" wave shapes and are given by $\phi_j = [\phi_{\mathtt{q}j}^{\mathtt{T}}\ \phi_{\mathtt{F}j}^{\mathtt{T}}]^{\mathtt{T}}$ where $\phi_{\mathtt{q}j}$ and $\phi_{\mathtt{F}j}$ are vectors of displacement and force components, respectively. Note that the transfer matrix $\mathbf{S}$ is symplectic, which means paired eigenvalues $(\mu_j, \mu_j^{\star} = 1/\mu_j)$, with $|\mu_j| < 1$, and therefore paired eigenvectors ϕ_j and $\phi_j^{\star}$ representing right-going and left-going waves, respectively. Also note that the computation of the eigenvalues and eigenvectors of $\mathbf{S}$ can be done via different strategies. The reader is referred to [9, 20, 19].

Within the WFE framework, the displacement and force vectors are expressed in terms of wave shape vectors. Thus the displacement and force vectors at a substructure interface (k), along a pipe, are expressed as [21]:

$$\mathbf{q}_{\mathtt{L}}^{(k)} = \mathbf{q}_{\mathtt{R}}^{(k)} = \mathbf{\Phi}_{\mathtt{q}}\mathbf{Q}^{(k)} + \mathbf{\Phi}_{\mathtt{q}}^{\star}\mathbf{Q}^{\star(k)}, \tag{8}$$

$$-\mathbf{F}_{\mathtt{L}}^{(k)} = \mathbf{F}_{\mathtt{R}}^{(k)} = \mathbf{\Phi}_{\mathtt{F}}\mathbf{Q}^{(k)} + \mathbf{\Phi}_{\mathtt{F}}^{\star}\mathbf{Q}^{\star(k)}, \tag{9}$$

where $\mathbf{\Phi}_{\mathtt{q}} = [\boldsymbol{\phi}_{\mathtt{q}1} \cdots \boldsymbol{\phi}_{\mathtt{q}n}]$, $\mathbf{\Phi}_{\mathtt{q}}^{\star} = [\boldsymbol{\phi}_{\mathtt{q}1}^{\star} \cdots \boldsymbol{\phi}_{\mathtt{q}n}^{\star}]$, $\mathbf{\Phi}_{\mathtt{F}} = [\boldsymbol{\phi}_{\mathtt{F}1} \cdots \boldsymbol{\phi}_{\mathtt{F}n}]$ and $\mathbf{\Phi}_{\mathtt{F}}^{\star} = [\boldsymbol{\phi}_{\mathtt{F}1}^{\star} \cdots \boldsymbol{\phi}_{\mathtt{F}n}^{\star}]$ [21]; also, $\mathbf{Q}^{(k)}$ and $\mathbf{Q}^{\star(k)}$ are wave amplitude vectors. For a pipe with N substructures, it can be shown that $\mathbf{Q}^{(k)} = \boldsymbol{\mu}^{k-1}\mathbf{Q}$ and $\mathbf{Q}^{\star(k)} = \boldsymbol{\mu}^{N+1-k}\mathbf{Q}^{\star}$ where $\mathbf{Q} = \mathbf{Q}^{(1)}$ and $\mathbf{Q}^{\star} = \mathbf{Q}^{\star\,(N+1)}$ represent wave amplitude vectors at the left and right ends of the pipe (respectively); also, $\boldsymbol{\mu} = \mathtt{diag}\{\mu_j\}_{j=1}^{n}$ is the diagonal matrix of eigenvalues μ_j for the right-going waves. As a result, Eqs. (8) and (9) yield [19]:

$$\mathbf{q}_{\mathtt{L}}^{(k)} = \mathbf{q}_{\mathtt{R}}^{(k)} = \mathbf{\Phi}_{\mathtt{q}}\boldsymbol{\mu}^{k-1}\mathbf{Q} + \mathbf{\Phi}_{\mathtt{q}}^{\star}\boldsymbol{\mu}^{N+1-k}\mathbf{Q}^{\star} \qquad k = 1, \ldots, N+1, \tag{10}$$

$$-\mathbf{F}_{\mathtt{L}}^{(k)} = \mathbf{F}_{\mathtt{R}}^{(k)} = \mathbf{\Phi}_{\mathtt{F}}\boldsymbol{\mu}^{k-1}\mathbf{Q} + \mathbf{\Phi}_{\mathtt{F}}^{\star}\boldsymbol{\mu}^{N+1-k}\mathbf{Q}^{\star} \qquad k = 1, \ldots, N+1. \tag{11}$$

The wave-based modeling of pipes connected with coupling elements (joints, defects) follows from Eqs. (10) and (11) (see [21, 19] for further details).

2.2 Scattering matrix

The scattering matrix of a coupling element, that could be either a joint (`j`) or a defect (`d`), provides the reflection and transmission coefficients for the incoming waves. Its expression, for a joint and a defect

connecting three waveguides/pipes 1, 2 and 3 (see Fig. 2), is given as [11, 14]:

$$\mathbb{C}^{\mathtt{j}} = -\left(\mathbf{D}^{\mathtt{j}*}\begin{bmatrix}\mathcal{L}_1\boldsymbol{\Phi}_{\mathtt{q}}^{\star} & \mathbf{0}\\ \mathbf{0} & \mathcal{L}_2\boldsymbol{\Phi}_{\mathtt{q}}\end{bmatrix} + \begin{bmatrix}\mathcal{L}_1\boldsymbol{\Phi}_{\mathtt{F}}^{\star} & \mathbf{0}\\ \mathbf{0} & -\mathcal{L}_2\boldsymbol{\Phi}_{\mathtt{F}}\end{bmatrix}\right)^{-1} \times \left(\mathbf{D}^{\mathtt{j}*}\begin{bmatrix}\mathcal{L}_1\boldsymbol{\Phi}_{\mathtt{q}} & \mathbf{0}\\ \mathbf{0} & \mathcal{L}_2\boldsymbol{\Phi}_{\mathtt{q}}^{\star}\end{bmatrix} + \begin{bmatrix}\mathcal{L}_1\boldsymbol{\Phi}_{\mathtt{F}} & \mathbf{0}\\ \mathbf{0} & -\mathcal{L}_2\boldsymbol{\Phi}_{\mathtt{F}}^{\star}\end{bmatrix}\right), \tag{12}$$

and

$$\mathbb{C}^{\mathtt{d}} = -\left(\mathbf{D}^{\mathtt{d}*}\begin{bmatrix}\mathcal{L}_2\boldsymbol{\Phi}_{\mathtt{q}}^{\star} & \mathbf{0}\\ \mathbf{0} & \mathcal{L}_3\boldsymbol{\Phi}_{\mathtt{q}}\end{bmatrix} + \begin{bmatrix}\mathcal{L}_2\boldsymbol{\Phi}_{\mathtt{F}}^{\star} & \mathbf{0}\\ \mathbf{0} & -\mathcal{L}_3\boldsymbol{\Phi}_{\mathtt{F}}\end{bmatrix}\right)^{-1} \times \left(\mathbf{D}^{\mathtt{d}*}\begin{bmatrix}\mathcal{L}_2\boldsymbol{\Phi}_{\mathtt{q}} & \mathbf{0}\\ \mathbf{0} & \mathcal{L}_3\boldsymbol{\Phi}_{\mathtt{q}}^{\star}\end{bmatrix} + \begin{bmatrix}\mathcal{L}_2\boldsymbol{\Phi}_{\mathtt{F}} & \mathbf{0}\\ \mathbf{0} & -\mathcal{L}_3\boldsymbol{\Phi}_{\mathtt{F}}^{\star}\end{bmatrix}\right), \tag{13}$$

where $\mathbf{D}^{\mathtt{j}*}$ and $\mathbf{D}^{\mathtt{d}*}$ are the condensed DSMs of the joint and the defect which can be computed via the Craig-Bampton method [19, 22]; also, $\mathcal{L}_1$, $\mathcal{L}_2$ and $\mathcal{L}_3$ are direction cosine matrices which are introduced to project the local coordinate systems of the pipes onto a global reference one.

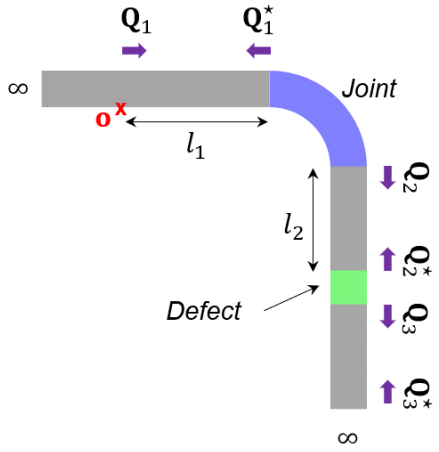

Figure 2: Three waveguides/pipes 1, 2 and 3 connected with a joint and a defect.

Let us denote by N_1, N_2 and N_3 the numbers of substructures of waveguides 1, 2 and 3 connecting the joint and the defect in Fig. 2. Thus, the wave amplitude vectors for the incoming and outgoing waves, at the boundaries of the joint/defect, can be related as follows:

$$\begin{bmatrix}\mathbf{Q}_1^{\star}\\ \mathbf{Q}_2\end{bmatrix} = \mathbb{C}^{\mathtt{j}}\begin{bmatrix}\boldsymbol{\mu}^{N_1}\mathbf{Q}_1\\ \boldsymbol{\mu}^{N_2}\mathbf{Q}_2^{\star}\end{bmatrix} = \begin{bmatrix}\mathbb{C}_{11}^{\mathtt{j}} & \mathbb{C}_{12}^{\mathtt{j}}\\ \mathbb{C}_{21}^{\mathtt{j}} & \mathbb{C}_{22}^{\mathtt{j}}\end{bmatrix}\begin{bmatrix}\boldsymbol{\mu}^{N_1}\mathbf{Q}_1\\ \boldsymbol{\mu}^{N_2}\mathbf{Q}_2^{\star}\end{bmatrix} \tag{14}$$

and

$$\begin{bmatrix}\mathbf{Q}_2^{\star}\\ \mathbf{Q}_3\end{bmatrix} = \mathbb{C}^{\mathtt{d}}\begin{bmatrix}\boldsymbol{\mu}^{N_2}\mathbf{Q}_2\\ \boldsymbol{\mu}^{N_3}\mathbf{Q}_3^{\star}\end{bmatrix} = \begin{bmatrix}\mathbb{C}_{22}^{\mathtt{d}} & \mathbb{C}_{23}^{\mathtt{d}}\\ \mathbb{C}_{32}^{\mathtt{d}} & \mathbb{C}_{33}^{\mathtt{d}}\end{bmatrix}\begin{bmatrix}\boldsymbol{\mu}^{N_2}\mathbf{Q}_2\\ \boldsymbol{\mu}^{N_3}\mathbf{Q}_3^{\star}\end{bmatrix}, \tag{15}$$

where $\mathbf{Q}_1^{\star}$ and $\mathbf{Q}_2$ (resp. $\mathbf{Q}_2^{\star}$ and $\mathbf{Q}_3$) are the wave amplitude vectors for the outgoing waves at the boundaries of the joint (resp. defect), see Fig. 2; also, $\boldsymbol{\mu}^{N_1}\mathbf{Q}_1$ and $\boldsymbol{\mu}^{N_2}\mathbf{Q}_2^{\star}$ (resp. $\boldsymbol{\mu}^{N_2}\mathbf{Q}_2$ and $\boldsymbol{\mu}^{N_3}\mathbf{Q}_3^{\star}$) are the wave amplitude vectors for the incoming waves at the same boundaries.

2.3 Times of flight

The group velocity c_{gj} for a wave j traveling in a certain pipe can be classically assessed from the dispersion curve $\omega \mapsto \Re\{\beta_j\}$ [23]:

$$c_{gj} = \frac{\partial \omega}{\partial \Re\{\beta_j\}}. \tag{16}$$

Alternatively, Eq. (16) can be written as:

$$c_{gj} = -d\frac{\partial \omega}{\partial \arg(\mu_j)}, \tag{17}$$

where μ_j is the wave parameter for the wave j, which is obtained via the WFE method (see Sec. 2.1). By considering the conventions defined earlier, it can be shown that the outgoing and incoming wave amplitude vectors at the left and right boundaries (k) and $(k+1)$ of a pipe substructure are related as follows:

$$\begin{bmatrix} \boldsymbol{\mu}^{N+1-k}\boldsymbol{Q}^{\star} \\ \boldsymbol{\mu}^{k}\boldsymbol{Q} \end{bmatrix} = \mathbb{C}^{\mathtt{s}} \begin{bmatrix} \boldsymbol{\mu}^{k-1}\boldsymbol{Q} \\ \boldsymbol{\mu}^{N-k}\boldsymbol{Q}^{\star} \end{bmatrix} = \begin{bmatrix} \mathbf{0} & \boldsymbol{\mu} \\ \boldsymbol{\mu} & \mathbf{0} \end{bmatrix} \begin{bmatrix} \boldsymbol{\mu}^{k-1}\boldsymbol{Q} \\ \boldsymbol{\mu}^{N-k}\boldsymbol{Q}^{\star} \end{bmatrix}. \tag{18}$$

Here, $\mathbb{C}^{\mathtt{s}}$ represents the scattering matrix of the substructure, with off-block diagonal terms representing diagonal matrices $\boldsymbol{\mu}$. This simply means that, for pure waveguides, waves are only subjected to transmission (coefficient μ_j) without wave conversion. Thus the time of flight taken for a wave j to get transmitted through a substructure can be obtained as:

$$\frac{d}{c_{gj}} = -\frac{\partial \arg(\mu_j)}{\partial \omega}. \tag{19}$$

Let us consider now a coupling element, between two pipes (e.g., pipes 1 and 2), inside which wave reflections and wave conversions are likely to occur. Following the same idea as Eq. (17), the time of flight in transmission for an incoming wave j in pipe 1 to be converted into an outgoing wave i in pipe 2 can be obtained as:

$$\tau_{ij} = -\frac{\partial \arg\left(\mathbb{C}_{21ij}\right)}{\partial \omega}, \tag{20}$$

where $\mathbb{C}_{21}$ is the transmission matrix between pipes 1 and 2. Also, the time of flight in reflection for an incoming wave j in pipe 1 to be converted into an outgoing wave i in pipe 1 can be obtained as:

$$\tau_{ij} = -\frac{\partial \arg\left(\mathbb{C}_{11ij}\right)}{\partial \omega}, \tag{21}$$

where $\mathbb{C}_{11}$ is the reflection matrix for the waves in pipe 1. Finally note that these times of flight τ_{ij} depend on the frequency of the waves which are considered.

2.4 Defect localization

A fitting procedure between the measured times of flight and the theoretical ones given in Sec. 2.3 allows the localization of a defect in a network of pipes. For the sake of clarity, let us consider an input wave packet l in pipe 1 which is (i) transmitted through a joint in pipe 2 (wave packet k), (ii) reflected by a defect in pipe 2 (wave packet j) and (iii) transmitted through the joint back to the measurement point in pipe 1 (wave packet i), see Fig. 2. Also, let us denote by τ_{ijkl} the measured time delay between the excitation time (wave packet l) and the measurement time (wave packet i). Then, by considering the theoretical expressions of the times of flight in Sec. 2.3, τ_{ijkl} can be decomposed as follows:

$$\tau_{ijkl} = \frac{l_1}{c_{gl}} + \tau_{kl}^{\mathtt{j}} + \frac{l_2}{c_{gk}} + \tau_{jk}^{\mathtt{d}} + \frac{l_2}{c_{gj}} + \tau_{ij}^{\mathtt{j}} + \frac{l_1}{c_{gi}}, \tag{22}$$

where $\tau_{kl}^{\mathtt{j}}$ and $\tau_{ij}^{\mathtt{j}}$ are the times of flight in transmission taken by wave packets l and j (respectively) to get across the joint, see Eq. (20). Also, $\tau_{jk}^{\mathtt{d}}$ is the time of flight in reflection for the defect, see Eq. (21). In the present case, l_1 is the distance between the measurement point and the joint, which is supposed to be known,

and l_2 is the distance between the joint and the defect, which is unknown. Also, in Eq. (22), l_1/c_{gi} and l_1/c_{gl} are the times of flight for wave packets i and l (respectively) to travel the distance l_1 in pipe 1, and l_2/c_{gj} and l_2/c_{gk} are the times of flight for wave packets j and k (respectively) to travel the distance l_2 in pipe 2. One should keep in mind that the group velocities c_{gi}, c_{gj}, c_{gk} and c_{gl} for waves in pipes can be easily obtained via the WFE method and the analysis of the related dispersion curves, see Sec. 2.3.

In this case, the sought distance l_2 can be estimated, from Eq. (22), as follows:

$$l_2 = \left(\tau_{ijkl} - \frac{l_1}{c_{gl}} - \tau_{kl}^{\mathsf{j}} - \tau_{jk}^{\mathsf{d}} - \tau_{ij}^{\mathsf{j}} - \frac{l_1}{c_{gi}} \right) \left(\frac{1}{c_{gk}} + \frac{1}{c_{gj}} \right)^{-1}. \tag{23}$$

It should be pointed that the expression of l_2 relies upon determining pathways $i \leftarrow j$, $j \leftarrow k$ and $k \leftarrow l$ taken by and incident wave packet l. There are, in fact, several possible pathways whose determination can be achieved in a pre-processing step by analyzing the components of the scattering matrices of the joint and the defect. Some of these are physically consistent and will all yield, in theory, the same solution l_2. Other pathways will give different solutions and must be discarded from the analysis (see next section).

3 Numerical results

Numerical simulations are carried out which concern the study of three pipes 1, 2 and 3 with a curved joint and a defect as shown in Fig. 2. Here, the curvature angle of the joint is 90^o, and the whole structure is supposed to lay on an elastic foundation. Schematics and FE meshes of the pipe substructures, defect and joint are shown in Fig. 3. The three pipes, the joint and the defect share the following properties: inner radius $R = 0.05$ m, thickness $h = 2.5$ mm, Young's modulus $E = 210$ GPa, density $\rho = 7800$ kg/m^3, Poisson's ratio $\nu = 0.3$, and damping coefficients $a = 10^{-3}$ s^{-1} and $b = 10^{-8}$ s, see Eq. (3). Here, the substructure length (pipes) is $d = 2.5$ mm. Also, the radius of curvature of the joint is $R^{\mathsf{j}} = 0.1$ m; as for the defect, it represents an assembly of 8 substructures (global length $d^{\mathsf{d}} = 0.02$ m) containing a small rectangular hole of length $l^{\mathsf{d}} = d = 2.5$ mm and an angle of aperture of 22.5^o as shown in Fig. 3(b,e).

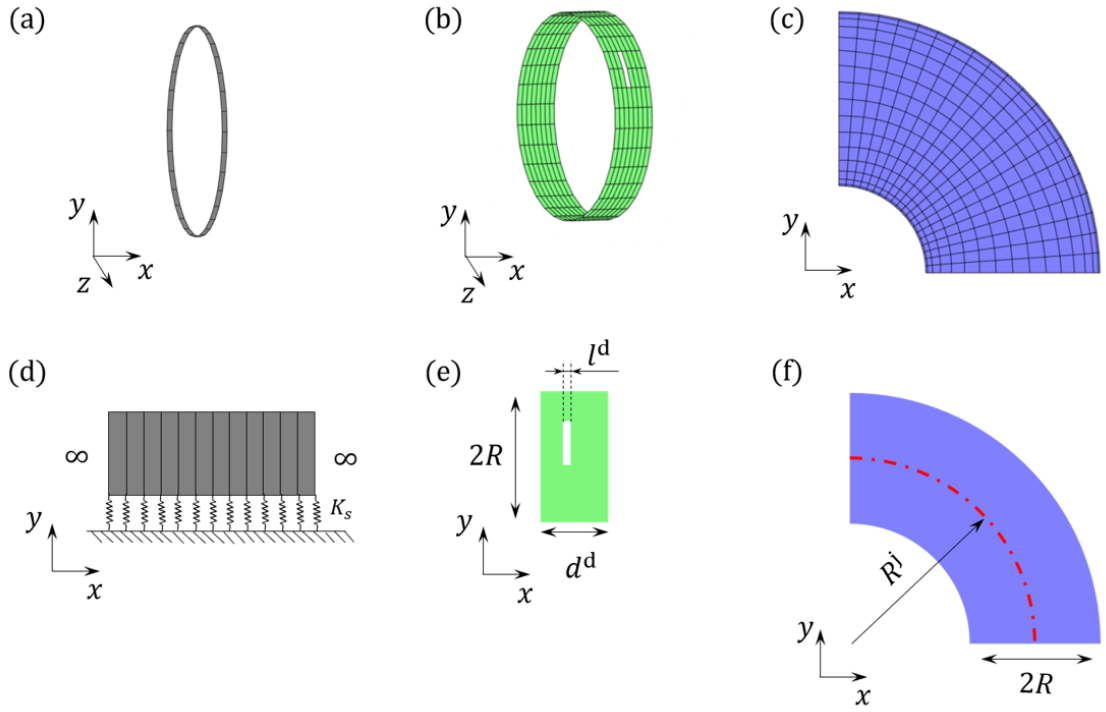

Figure 3: Schematic and FE meshes of (a) a pipe substructure, (b,e) the defect, (c,f) the joint, (d) a pipe on an elastic foundation.

The pipe substructures, the joint and the defect are modeled using "S4R" 4-node rectangular elements (ABAQUS) with 6 DOFs per node. The pipe substructures are meshed with 32 elements around the circumference, and 1 element along the length. Also, the joint is meshed using 32 elements around the circumference, and 20 elements around the curvature. Finally, the defect is meshed using 254 elements with 32 elements around the circumference and a lack of two elements for modeling the hole. Finally, the elastic foundation is modeled via periodic supports of stiffness $K_s = 10^8$N (vertical direction) at the bottom nodes of the whole structure.

The dispersion curves of the traveling waves in the pipes can be obtained via the WFE method (see Sec. 2.1) as shown in Fig. 4. Here, those associated with "low-order" right-going waves are displayed over the frequency band $[\,0, 40]$ kHz. Fig. 4(a) shows the real and imaginary parts of $\beta_j d$ (β_j and d being the wavenumbers and the substructure length, respectively), and Fig. 4(b) shows the related group velocities. These dispersion curves appear quite different to the usual ones in pipes, which is explained by the fact that an elastic foundation is added. Here, the fundamental torsional wave mode $\mathtt{T}(0,1)$, which is non-dispersive, is highlighted together with low-order dispersive non-axisymmetric flexural wave modes $\mathtt{F}(1,2)$, $\mathtt{F}(1,3)$ and $\mathtt{F}(2,2)$, and low-order longitudinal wave modes (see blue, yellow and purple curves). As explained earlier, wave mode conversion among these waves is likely to occur inside the joint and the defect (transmission, reflection).

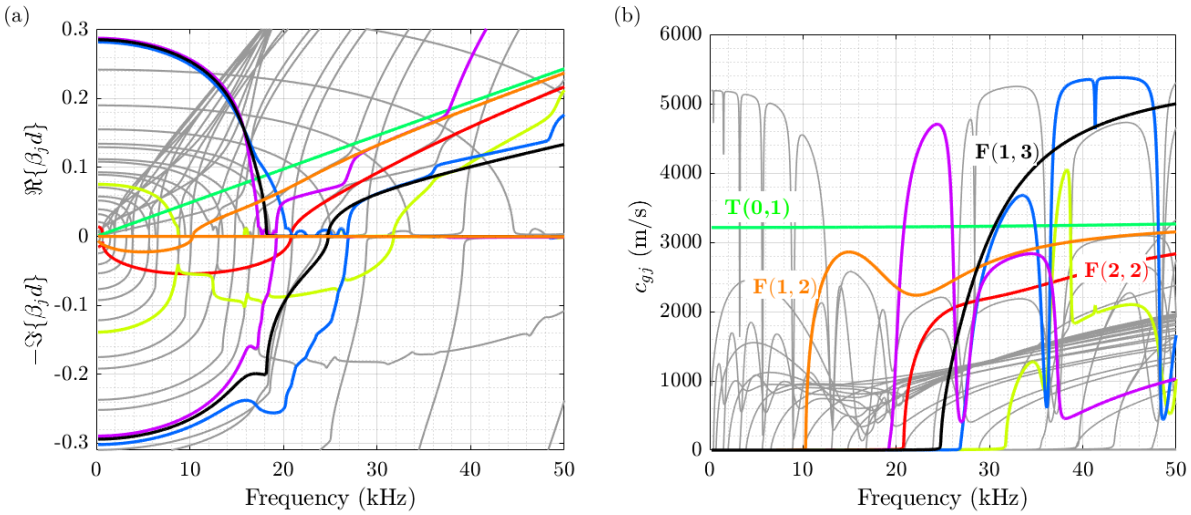

Figure 4: (a) Wavenumbers $\beta_j d$ (real and imaginary parts) and (b) group velocities: (green line) torsional mode $\mathtt{T}(0,1)$, (orange line) flexural mode $\mathtt{F}(1,2)$; (black line) flexural mode $\mathtt{F}(1,3)$; (red line) flexural mode $\mathtt{F}(2,2)$; (blue, yellow and purple lines) longitudinal modes.

The time response of the pipe assembly is investigated, with an input excitation/measurement point in pipe 1 at a distance $l_1 = 10$ m from the joint, see Fig. 2. The distance between the joint and the defect is $l_2 = 10$ m, which also represents the length of pipe 2. Here, both pipes 1 and 3 are supposed to be semi-infinite. An input Gaussian pulse centered at 30 kHz representing a right-going wave packet "$\mathtt{T}(0,1)$" is considered as shown in Fig. 5. The problem is solved in the frequency domain with the WFE method (see [19] for the methodology), and the time response is obtained via an inverse Fourier transform of the frequency response [24].

Fig. 6 shows the normalized reflected wave packets (vertical displacement) at the measurement point. Here, five wave packets of $\mathtt{T}(0,1)$-type are observed. These result from reflection at the joint (wave packet (1)) and reflection at the defect via transmission through the joint (wave packets (2), (3), (4) and (5)). Wave packets (2)-(5) are associated to different pathways and different wave conversions inside the joint and the defect, as reported earlier. This illustrates the difficulty to localize a defect after a joint, i.e., given the occurrence of different wave pathways for a given type of input/output wave. It should be recalled, again, that these pathways, for an input wave packet, are to be understood as the different possible wave packets which are

transmitted through the joint in pipe 2, reflected via the defect in the same pipe, and transmitted via the joint back to the measurement point.

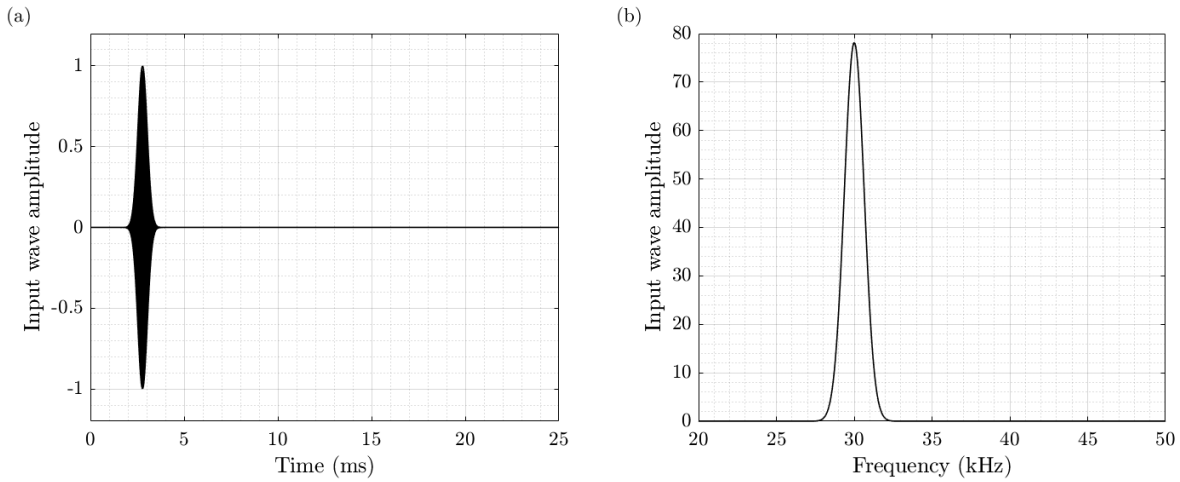

Figure 5: (a) Pulse excitation in the time domain and (b) absolute value of the related Fourier transform.

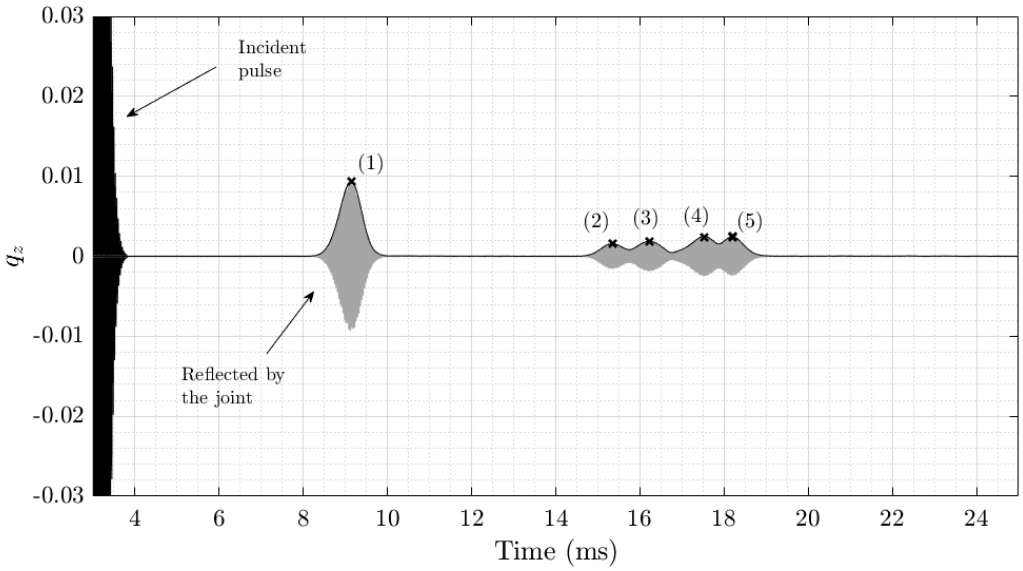

Figure 6: Reflected wave packets at the measurement point: (1) wave packet reflected by the joint; (2)-(5) wavepackets issued from the defect. Dark crosses highlight the tips of the wave packets.

An analysis of the components of the scattering matrices of the joint and the defect can help identify these different pathways. For instance, the transmission coefficients for the incident wave $\mathtt{T}(0,1)$ through the joint are shown in Fig. 7(a). Here, the waves which are likely to be generated in pipe 2 — i.e., those with the highest transmission coefficient at 30 kHz — are highlighted by colored curves. For instance, the red curve represents the transmission coefficient from wave $\mathtt{T}(0,1)$ to wave $\mathtt{F}(2,2)$, and the green curve represents the transmission coefficient from wave $\mathtt{T}(0,1)$ to wave $\mathtt{T}(0,1)$. Also, by analyzing the reflection coefficients at the defect, several possible pathways can be postulated. Some of these are physical, others are not.

To identify the physical pathways as well as the sought position of the defect $l_2 = 10$ m, the following strategy can be proposed. The idea is that, for a certain measured time of flight τ_{ijkl}, different physical pathways should give the same estimate of l_2. Fig. 7(b) shows the variation of τ_{ijkl} against the length l_2, as proposed by Eq. (22), for different pathways. Also, the measured times of flight, for the reflected

wave packets, are shown via horizontal dashed lines in Fig. 7(b). By intersecting the resulting oblique and horizontal lines, a clear match with $l_2 = 10$ m can be obtained for three pathways. Other pathways may give wrong result — i.e., the purple curve in Fig. 7(b) — which means that they do not physically happened.

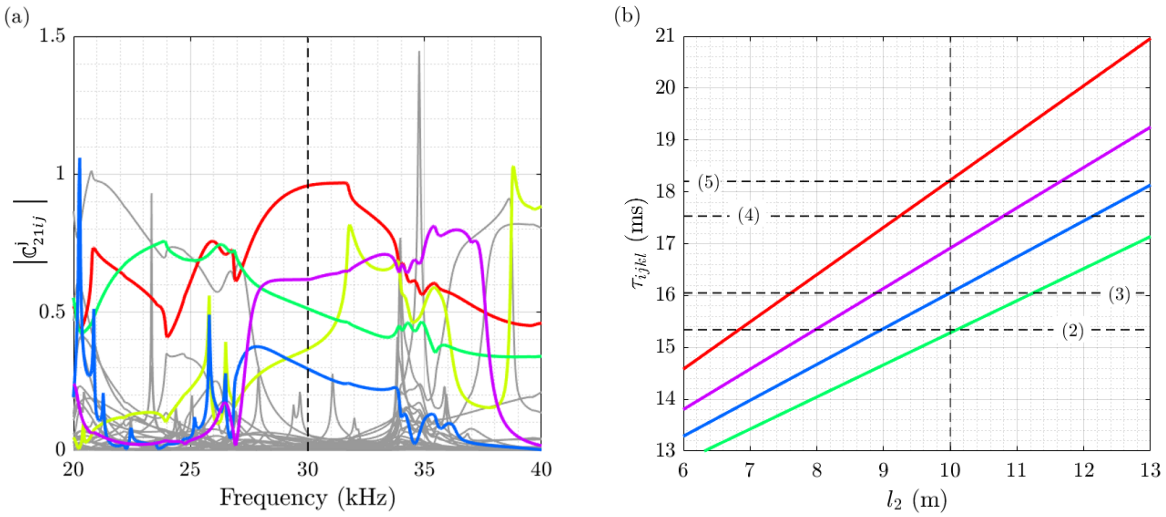

Figure 7: (a) Transmission coefficients for the incident wave $\mathtt{T}(0,1)$ through the joint; highest coefficients at 30 kHz are highlighted by colored curves. (b) Times of flight τ_{ijkl} as functions of the length l_2, for different pathways; measured times of flight are highlighted by horizontal dashed lines.

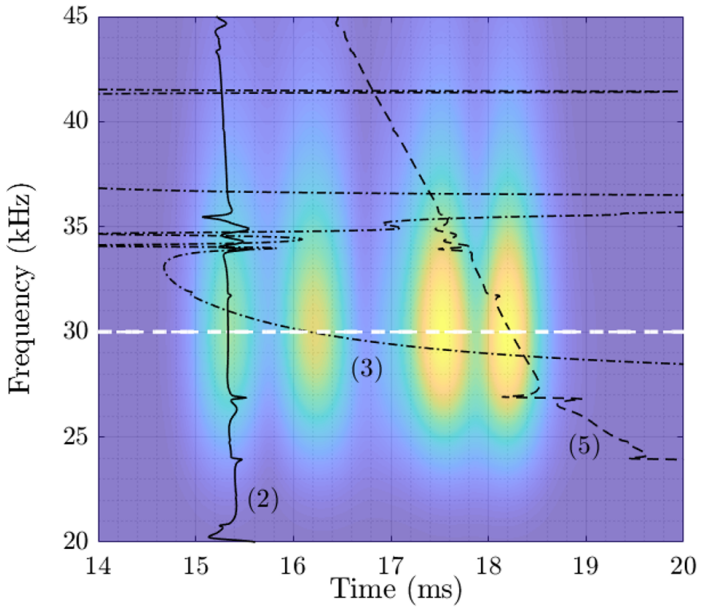

Figure 8: Frequency-time map of the reflected waves issued from the defect. Measured times of flight are highlighted by yellow spots. Estimated times of flight represent the crossing points between the black curves and the white dashed line.

Accurate estimates of the position of the defect l_2 can be obtained from Eq. (23), i.e., from the measured times of flight τ_{ijkl} and several identified pathways (2), (3) and (5). Results are shown in Tab. 1, where "$\mathtt{H.O.}$" means high-order wave modes. In this case, the position of the defect can be identified with an error smaller than 1%. This also highlights the robustness of the proposed approach in the sense that the localization of the defect can be accurately determined regardless of the pathway analyzed.

Table 1: Estimated position of the defect from Eq. (23), and relative error (reference is $l_2 = 10$ m).

	$ijkl$	τ_{ijkl} (ms)	l_2 (m)	Relative error (%)
(2)	$\mathtt{T}(0,1) \leftarrow \mathtt{T}(0,1) \leftarrow \mathtt{T}(0,1) \leftarrow \mathtt{T}(0,1)$	15.34	10.09	0.9
(3)	$\mathtt{T}(0,1) \leftarrow \mathtt{H.O.} \leftarrow \mathtt{H.O.} \leftarrow \mathtt{T}(0,1)$	16.05	9.99	0.1
(5)	$\mathtt{T}(0,1) \leftarrow \mathtt{F}(2,2) \leftarrow \mathtt{F}(2,2) \leftarrow \mathtt{T}(0,1)$	18.20	10.08	0.8

To further investigate the proposed approach, a frequency-time map of the measured reflected signals can be considered as shown in Fig. 8. Here, the yellow spots highlight the measured reflected signals. Also, the black curves represent the theoretical times of flight for different pathways (2), (3) and (5), see Eq. (22). Otherwise, in Fig. 8, the white horizontal curve at 30 kHz represent the excitation frequency. This procedure allows a verification of the pathways identified via Fig. 7(b). For these pathways indeed, one can check that the intersection points between the black curves and the white one perfectly match with the center of the yellow spots, i.e., with the tips of the reflected signals shown in Fig. 6.

Fig. 8 provides additional information about the reflected times of flight. For instance, the black curves contain sharp horizontal peaks at some particular frequencies. This phenomenon would penalize the detection of reflected wave packets — e.g., the one corresponding to a certain pathway — which is explained by the difficulty to determine the crossing points between these curves and a white one positioned at these frequencies. Such a behavior occurs at the resonances frequencies of the coupling elements (joint, defect) or at the cut-on frequencies of the waves where the group velocities exhibit a singular behavior. Input wave packets at these frequencies are likely to induce reflected signals which are spread in time, which as such make these excitation frequencies not suitable to localize the defect. It should be emphasized that this issue is not linked to numerical modeling, but results from physical phenomena. It is therefore advised to consider different values of excitation frequencies. The proposed WFE approach could be advantageously considered to quickly select these excitation frequencies in a pre-processing step.

4 Conclusion

In this paper, a WFE strategy has been proposed to localize defects in networks of pipes. The strategy involves estimating the times of flight for waves transmitted through, or reflected by, a curved joint and a defect. In the proposed approach, the times of flight are defined from the frequency derivatives of the arguments of the scattering matrix of a coupling element. By considering these times of flight together with those associated with the propagation of waves in pipes, it becomes possible from measured time signals to identify a defect. This also provides a physical insight into the natures of the waves which are truly transmitted through a joint and reflected by a defect (pathways). Numerical experiments have been proposed concerning the analysis of three pipes with a curved joint and a defect of small size.

References

[1] J. L. Rose, "A Baseline and Vision of Ultrasonic Guided Wave Inspection Potential," *Journal of Pressure Vessel Technology*, vol. 124, no. 3, p. 273, 2002.

[2] A. G. Every, M. Y. Shatalov, and A. S. Yenwong-Fai, "Progress in the analysis of non-axisymmetric wave propagation in a homogeneous solid circular cylinder of a piezoelectric transversely isotropic material," *Physics Procedia*, vol. 3, no. 1, pp. 473–479, 2010, international Congress on Ultrasonics, Santiago de Chile, January 2009.

[3] D. C. Gazis, "Three-dimensional investigation of the propagation of waves in hollow circular cylinders. i. analytical foundation," *The Journal of the Acoustical Society of America*, vol. 31, no. 5, pp. 568–573, 1959.

[4] J. Zemanek, "An experimental and theoretical investigation of elastic wave propagation in a cylinder," *The Journal of the Acoustical Society of America*, vol. 51, no. 1B, pp. 265–283, 1972.

[5] A. Demma, P. Cawley, M. Lowe, and B. Pavlakovic, "The Effect of Bends on the Propagation of Guided Waves in Pipes," *Journal of Pressure Vessel Technology*, vol. 127, p. 328, 2005.

[6] T. Hayashi, K. Kawashima, Z. Sun, and J. L. Rose, "Guided Wave Propagation Mechanics Across a Pipe Elbow," *Journal of Pressure Vessel Technology*, vol. 127, no. 3, pp. 322–327, 01 2005.

[7] R. M. Sanderson, D. A. Hutchins, D. R. Billson, and P. J. Mudge, "The investigation of guided wave propagation around a pipe bend using an analytical modeling approach," *The Journal of the Acoustical Society of America*, vol. 133, 2013.

[8] J. Ni, S. Zhou, P. Zhang, and Y. Li, "Effect of pipe bend configuration on guided waves-based defects detection: An experimental study," *Journal of Pressure Vessel Technology, Transactions of the ASME*, vol. 138, 2015.

[9] W. X. Zhong and F. W. Williams, "On the Direct Solution of Wave Propagation for Repetitive Structures," *Journal of Sound and Vibration*, vol. 181, no. 3, pp. 485–501, 1995.

[10] D. Mead, "A general theory of harmonic wave propagation in linear periodic systems with multiple coupling," *Journal of Sound and Vibration*, vol. 27, no. 2, pp. 235–260, Mar. 1973.

[11] J.-M. Mencik and M. N. Ichchou, "Multi-mode propagation and diffusion in structures through finite elements," *European Journal of Mechanics, A/Solids*, vol. 24, no. 5, pp. 877–898, 2005.

[12] W. J. Zhou and M. N. Ichchou, "Wave propagation in mechanical waveguide with curved members using wave finite element solution," *Computer Methods in Applied Mechanics and Engineering*, vol. 199, 2010.

[13] W. J. Zhou and M. N. Ichchou, "Wave scattering by local defect in structural waveguide through wave finite element method," *Structural Health Monitoring*, vol. 10, pp. 335–349, 2011.

[14] M. N. Ichchou, J.-M. Mencik, and W. Zhou, "Wave finite elements for low and mid-frequency description of coupled structures with damage," *Computer Methods in Applied Mechanics and Engineering*, vol. 198, no. 15-16, pp. 1311–1326, 2009.

[15] M. Kharrat, M. N. Ichchou, O. Bareille, and W. Zhou, "Wave Diffusion Sensitivity to Angular Positions of Defects in Pipes," *Journal of Computational Acoustics*, vol. 23, no. 03, p. 1550013, Sep. 2015.

[16] W. J. Zhou, M. N. Ichchou, and J.-M. Mencik, "Analysis of wave propagation in cylindrical pipes with local inhomogeneities," *Journal of Sound and Vibration*, vol. 319, no. 1-2, pp. 335–354, 2009.

[17] V. Denis and J. M. Mencik, "A wave-based optimization approach of curved joints for improved defect detection in waveguide assemblies," *Journal of Sound and Vibration*, vol. 465, 2020.

[18] C. Schaal, S. Bischoff, and L. Gaul, "Damage detection in multi-wire cables using guided ultrasonic waves," *Structural Health Monitoring: An International Journal*, vol. 15, no. 3, pp. 279–288, 2016.

[19] J.-M. Mencik, "New advances in the forced response computation of periodic structures using the wave finite element (WFE) method," *Computational Mechanics*, vol. 54, no. 3, pp. 789–801, 2014.

[20] J.-M. Mencik and D. Duhamel, "A wave-based model reduction technique for the description of the dynamic behavior of periodic structures involving arbitrary-shaped substructures and large-sized finite element models," *Finite Elements in Analysis and Design*, vol. 101, pp. 1–14, 2015.

[21] J.-M. Mencik, "On the low- and mid-frequency forced response of elastic structures using wave finite elements with one-dimensional propagation," *Computers & Structures*, vol. 88, no. 11-12, pp. 674–689, Jun. 2010.

[22] P. B. Silva, J.-M. Mencik, and J. R. F. Arruda, "Wave finite element-based superelements for forced response analysis of coupled systems via dynamic substructuring," *International Journal for Numerical Methods in Engineering*, vol. 107, no. 6, pp. 453–476, 2015.

[23] B. A. Auld and R. E. Green, "Acoustic fields and waves in solids: Two volumes," *Physics Today*, vol. 27, 1974.

[24] A. Marzani, "Time–transient response for ultrasonic guided waves propagating in damped cylinders," *International Journal of Solids and Structures*, vol. 45, no. 25-26, pp. 6347–6368, Dec. 2008.